12-2011

Physics and Statistics of Non-Ohmic Shunt Conduction and Metastability in Amorphous Silicon p-i-n Solar Cells

Sourabh Dongaonkar
Purdue University - Main Campus, sourabh@purdue.edu

karthik Yogendra
Indian Institute of Technology - Bombay

Souvik Mahapatra
Indian Institute of Technology - Bombay

Muhammad A. Alam
Purdue University

Dongaonkar, Sourabh; Yogendra, karthik; Mahapatra, Souvik; and Alam, Muhammad A., "Physics and Statistics of Non-Ohmic Shunt Conduction and Metastability in Amorphous Silicon p-i-n Solar Cells" (2011). *Birck and NCN Publications.* Paper 812.
http://dx.doi.org/10.1109/JPHOTOV.2011.2174030

Physics and Statistics of Non-Ohmic Shunt Conduction and Metastability in Amorphous Silicon p–i–n Solar Cells

Sourabh Dongaonkar, Karthik Y., Souvik Mahapatra, *Senior Member, IEEE*, and Muhammad A. Alam, *Fellow, IEEE*

***Abstract*—In this paper, we present a physical model of the non-Ohmic shunt current $I_{\rm SH}$ in amorphous silicon (a-Si:H) p–i–n solar cells and validate it with detailed measurements. This model is based on space-charge-limited (SCL) transport through localized p–i–p shunt paths. These paths can arise from n-contact metal incorporation in the a-Si:H layer, causing the (n)a-Si:H to be counterdoped to p-type. The model not only explains all the electrical characteristics of preexisting shunts but also provides insight into the metastable switching that is observed in the shunt-dominated region of dark current as well. We first verify the SCL model using simulations and statistically robust measurements, and then use it to analyze our systematic observations of nonvolatile switching of the low-bias dark characteristics. This study interprets broad experimental observations regarding shunt behavior, and suggests possible techniques for alleviating shunt-induced performance and reliability issues.**

***Index Terms*—Amorphous silicon, photovoltaic (PV) cells, shunt, thin films.**

I. Introduction

IMPROVEMENT of parametric yield, through the reduction of process variability, is critical for the commercial success of thin-film photovoltaic (PV) technologies [1]. One of the most important variability concerns is variable shunt leakage in solar cells. It has been identified as one of the major factors responsible for the significant gap between panel and cell efficiencies [2], [3]. Despite its importance in determining the panel output, the physics of shunt formation is not as well understood as that of the solar cell itself, and most studies of $I_{\rm SH}$ are empirical in nature. Some shunts at the panel level have been correlated with localized, macroscopic (up to millimeters) nonuniformities (e.g., pinholes), which are caused by particulate debris on the panel surface [3], [4]. These "extrinsic" shunts can be minimized by the better control of deposition conditions. However, significant shunt currents are observed even in cells fabricated with excellent process control, which are generally free from the "extrinsic" defects. These "intrinsic" shunts cannot be traced to any visible defect on the surface but show up in dark lock-in thermography images as bright spots [4].

The intrinsic shunts introduce considerable performance variation among nominally identical cells, and in this paper, we will focus on the physical mechanisms of their formation, conduction, and nonvolatile switching. We find that unlike the Ohmic extrinsic shunts, the intrinsic shunts show *non-Ohmic* voltage dependence [5]. Moreover, these shunt currents also show an abrupt threshold switching behavior on application of reverse voltages [6], [7]. This threshold switching is known in the PV industry and is used for electrical shunt removal/reduction (shunt busting) [8]. However, we find that the switching behavior is actually metastable, and cell $I_{\rm SH}$ can also *increase* on application of reverse bias. This has important implications for long-term panel reliability, because during normal operation, partial shadows on the panel can result in moderate-to-high reverse bias stress across shaded cells. And, any resulting increase in the shunt current because of this metastability can have a significant impact on the long-term panel output [9]. Therefore, understanding the formation of these shunts during fabrication and their metastability because of reverse bias is of great importance for design and development of a-Si:H PV technology. The goal of this paper is the development of such a model, which can lead to strategies for the reduction of the shunt loss in a-Si:H cells.

II. Space-Charge-Limited Shunt Current

A. Phenomenological Model

The identification of shunt conduction mechanism in as-fabricated a-Si:H solar cells is the critical first step in the development of a physical picture. We observed that $I_{\rm SH}$, in a-Si:H cells, is characterized by three key empirical features, namely symmetry of shunt current about $V = 0$, non-Ohmic power-law voltage dependence $I \sim V^{\beta}$ [see Fig. 1(a)], and weak temperature dependence [see Fig. 1(b)] compared to the temperature-activated diode current component.

We had proposed a phenomenological space-charge-limited (SCL) current model to account for these features within a coherent framework [5]. SCL transport features single-carrier transport in a symmetric (e.g., metal/semiconductor/metal type)

Manuscript received June 27, 2011; revised August 5, 2011; accepted October 18, 2011. This work was supported by Semiconductor Research Corporation, Energy Research Initiative (SRC-ERI) Network for Photovoltaic technology. The work of M. A. Alam was the supported in part by the Center for Redefining Photovoltaic Efficiency through Molecule Scale Control, which is an Energy Frontier Research Center funded by the U.S. Department of Energy, Office of Science, under Award DE-SC0001085.

S. Dongaonkar and M. A. Alam are with the School of Electrical and Computer Engineering, Purdue University, West Lafayette, IN 47906 USA (e-mail: sourabh@purdue.edu; alam@purdue.edu).

Karthik Y. and S. Mahapatra are with the Department of Electrical Engineering, Indian Institute of Technology Bombay, Mumbai 400076, India (e-mail: karthiky@ee.iitb.ac.in; souvik@ee.iitb.ac.in).

Color versions of one or more of the figures in this paper are available online at http://ieeexplore.ieee.org.

Digital Object Identifier 10.1109/JPHOTOV.2011.2174030

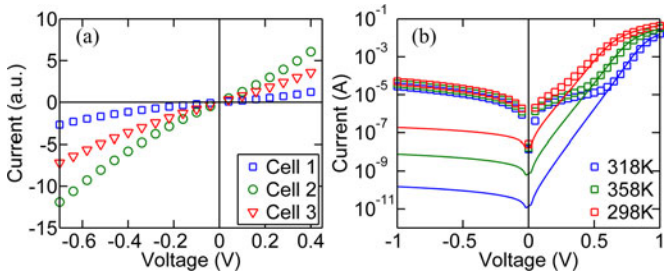

Fig. 1. (a) Symmetric non-Ohmic behavior about $V = 0$ for three (symbols) nominally identical devices (scaled for clarity). (b) Temperature-dependent dark *IV* characteristics showing weak temperature dependence of $I_{\rm SH}$ (symbols, below 0.5 V), compared with the activated diode current (solid lines).

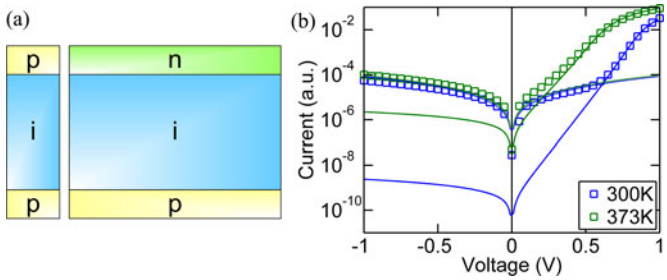

Fig. 3. (a) Separation of diode and shunt path allows simplification to 1-D structures. (b) One-dimensional simulations of shunt (dashed line) and diode (solid line) showing excellent match with dark *IV*-T data (symbols).

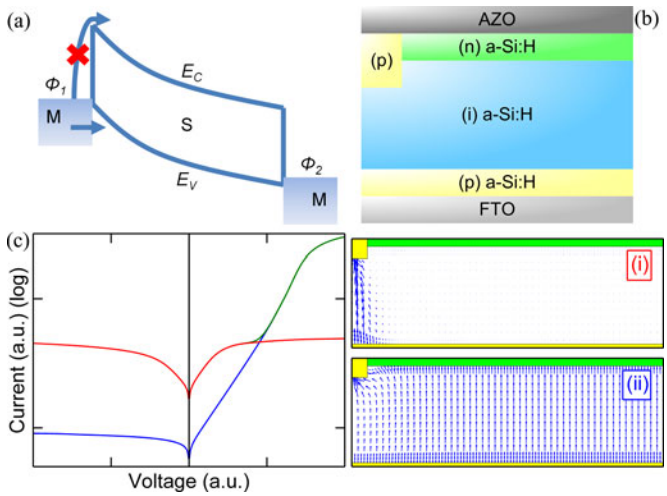

Fig. 2. (a) Symmetric MSM structure for SCL conduction showing single-carrier (hole) injection. (b) Proposed localized parasitic p–i–p structure on the left of otherwise ideal p–i–n structure. (c) Dark *IV* characteristics obtained from the 2-D simulation of the structure in (b), showing that the shunt (red) and diode (blue) currents dominate in different voltage regimes to give the total dark current (green). Quiver plots contrast localized current conduction in the p-i-p region (i) at low biases with the uniform diode current conduction (ii) at higher biases.

structure [see Fig. 2(a)], with the general form

$$I_{\rm SCL} = A\varepsilon\mu_c(\gamma)\frac{V^{\gamma+1}}{L^{2\gamma+1}}. \quad (1)$$

Here, A is the area, L is the thickness, ε is the dielectric constant, $\mu_c(\gamma)$ is the effective carrier mobility, and parameter γ is a function of trap distribution inside the band gap [10]. It is apparent from (1) that symmetry and non-Ohmic nature of $I_{\rm SH}$ can be explained readily by SCL conduction. And, since the only temperature-dependent term in (1) is mobility, which is a weak function of temperature [11], the temperature dependence of $I_{\rm SH}$ is also weak. While the electrical features of $I_{\rm SH}$ can be understood from (1), the physical nature of shunt paths that are responsible for SCL conduction requires further analysis.

B. Localized p–i–p Shunt Hypothesis

We now investigate a likely physical origin of the symmetric parasitic path that is responsible for an SCL shunt path. We propose that the parallel, symmetric shunt path is formed as a localized p–i–p structure [see Fig. 2(b)]. For a typical a-Si:H p–i–n cell that is deposited on fluorinated tin oxide (FTO) substrate, with aluminum-doped zinc oxide (AZO) top contact, such a path might form during cell fabrication, because of a local incursion of Al from the top AZO contact in the a-Si:H layer. This would result in a localized current path, in parallel to the bulk exponential diode current. This localized p-i-p shunt hypothesis can be explored by numerical simulation. A self-consistent simulation of the 2-D structure in Fig. 2(b), using commercial Synopsys Medici software, readily reproduces the essential features of the SCL shunt [see Fig 2(c)]. The SCL current through the p–i–p shunt region dominates in the lower bias regimes, while the exponential diode current through the p–i–n region takes over at higher forward biases. This transition can be visualized using the quiver plots of the current in Fig. 2(c). As shown in (i), the current is localized to the p–i–p shunt region. At higher forward biases however, the p–i–n diode current takes over and the current distribution becomes more uniform across the bulk device, as shown in (ii).

Another useful insight from the quiver plots is that the shunt and diode currents are spatially separated and dominate the conduction in different voltage ranges. Therefore, we can avoid the computationally intensive 2-D simulations by the simulation of the 1-D p–i–p shunt and p–i–n diode separately [see Fig. 3(a)]. The total current is, then, given by $I_{\rm Dark} = A_{\rm cell}J_{\rm pin} + A_{\rm shunt}J_{\rm pip}$. Here, $A_{\rm cell}$ is the cell area, and $A_{\rm shunt}$ is the sum of all shunt areas in a particular cell. Typically, we find $A_{\rm shunt} \approx 10^{-4}$–$10^{-6}A_{\rm cell}$, which is also consistent with the spot sizes in thermography images from the literature [12]. In Fig. 3(b), we show that a 1-D simulation of the p–i–p shunt and p–i–n diode matches the measured voltage and temperature dependences of the dark *IV* characteristics of the cell very well.

C. Formation of Preexisting Shunts

The most likely cause of p–i–p shunt formation during cell fabrication is that Al from the top AZO layer diffuses into the (n)a-Si:H and counterdopes it to p-type [13]. Since the n-layer is only ~20 nm thick, even a small Al incursion can result in a local p–i–p shunt path, which can occur in areas of AZO grain boundaries or regions of high void density in a-Si:H. Diffusion of Al in a-Si:H is a known concern for cell stability, because it can diffuse inside a-Si:H at relatively low temperatures (200–300°C) [13]. Therefore, it seems likely that during sputtering of

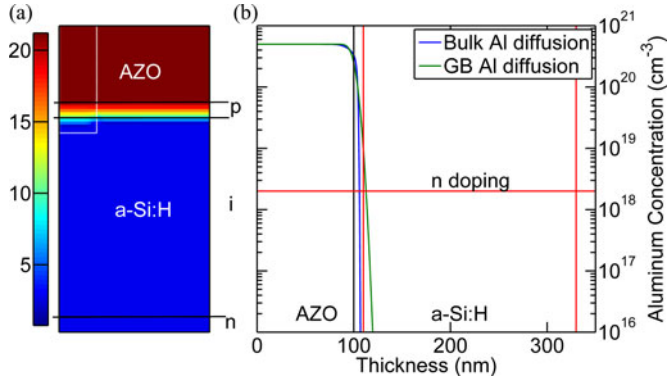

Fig. 4. (a) Two-dimensional simulation of Al diffusion during sputtering of top contact showing enhanced Al incorporation near the AZO grain boundary (dotted box). (b) One-dimensional plot of Al profiles show that the Al diffusion can overcome n-doping near grain boundary regions.

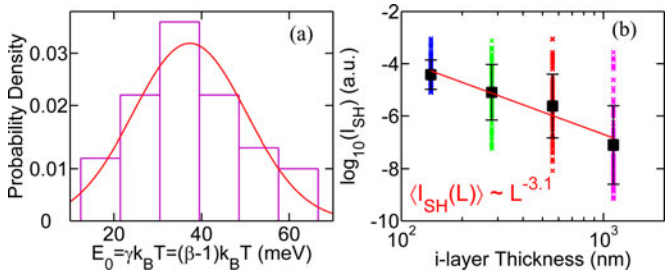

Fig. 5. (a) Extracted characteristic slope of band tails E_0 is ∼40 meV for 61 devices, which is very close to the valence band tail slope in a-Si:H, as expected from the p-i-p shunt hypothesis. (b) Thickness dependence of the shunt current (at −2 V) shows the inverse power law predicted by the SCL model; the crosses represent individual cells, and squares are geometric means with the error bars denoting the standard deviation.

the top contact, Al may diffuse to sufficient depths (>20 nm) and destroy the n–i junction at some locations to form a parasitic shunt. Al migration is facilitated by vacancies that are created by diffusion of Si to AZO, especially at AZO grain boundaries. We simulated this interdiffusion of Si and Al, for moderate deposition temperatures and times, using reported values [14]. The diffusion coefficient of Al was enhanced based on the Si vacancy concentration. In Fig. 4(a), we show the results of this 2-D simulation, showing that Al can indeed reach past the n–i junction, especially near AZO grain boundaries, where Si diffusivity is increased. The extent of Al incursion can be significant to overcome the n–i junction at the grain boundary regions, as seen in Fig. 4(b). This simulation shows that a good approach to curb shunt formation would be reducing Al diffusion, possibly through the introduction of a barrier layer. Care must be taken however, to minimize any extra series resistance, which may be introduced by the diffusion barrier.

III. Validation of the p–i–p Shunt Model

While electrical features are reproduced well by the localized p–i–p shunt model, a conclusive confirmation of the model requires that its predictions be verified independently. Therefore, in the next sub-sections we investigate two important predictions of the SCL model with statistically robust measurements.

A. Confirmation of Hole Transport

SCL conduction requires single-carrier injection, and in the case of p–i–p shunt, holes that are injected in the i-layer will dominate the transport. We can indirectly establish the dominance of hole transport in $I_{\rm SH}$ by examining the power exponent, i.e., $\beta = \gamma+1$, of SCL conduction in (1). For the SCL current in materials with exponentially distributed shallow traps, it has been shown that the parameter $\gamma = E_0/k_BT$, where E_0 is the characteristic energy of the trap distribution [10]. This feature of SCL current is well known and has previously been used to characterize the shallow band-tail states in a-Si:H [15]. Using this approach, we calculate the characteristic energy E_0 from the measured shunt current of 61 cells and find it to be about 40 meV [see Fig. 5(a)]. Note that the characteristic slope of the valence band tail in a-Si:H is ∼40 meV, as opposed to the conduction band-tail slope of ∼20 meV [16]. This confirms that the SCL shunt current is indeed because of injection of holes in the i-layer, which is consistent with the hypothesis of the p–i–p shunt.

B. Thickness Dependence

Another prediction of the SCL shunt current expression from (1) is that $I_{\rm SH}$ scales inversely with semiconductor layer thickness as a power law, i.e., $I_{\rm SCL} \sim 1/L^{2\gamma+1}$. To check this prediction, we measured 356 devices with i-layer thicknesses 140, 280, 560, and 1120 nm (89 devices each). In Fig. 5(b), the dark current at −2 V (shunt-dominated region) versus the i-layer thickness is plotted for all measured devices. Here, each dot represents a separate device; the symbols are the geometric means with error bars showing the standard deviation. We find that the geometric mean of the data indeed shows a power-law behavior, with the power exponent ∼−2.8, broadly consistent with the SCL model. This statistically robust trend affirms the second prediction of the proposed p–i–p shunt model.

IV. Statistics of Shunt Formation

The large spread in the shunt-current magnitude, which is shown in Fig. 5(b), raises interesting questions about distribution of shunts on the cell surface. If we plot the shunt-current magnitudes (dark current at −2 V) for the different i-layer thicknesses on a probability plot, as shown in Fig. 6(a), we find that the empirical distribution generally shows lognormal characteristics. Note that the lognormal lines describe the $I_{\rm SH}$ data very well for the i-layer thicknesses of 280 and 560 nm. The deviation from lognormal for 1120 nm case reflects contamination due to the lower limit of measurement accuracy of ∼100 pA. Therefore, the distribution shows a sharp cutoff near 100 pA value. On the other hand, for 140 nm case the reverse diode current is large enough to contaminate $I_{\rm SH}$, presumably due to enhanced tunneling [17]. On the removal of those contaminated data points, we find that $I_{\rm SH}$ for all layer thicknesses follows the lognormal distribution very closely

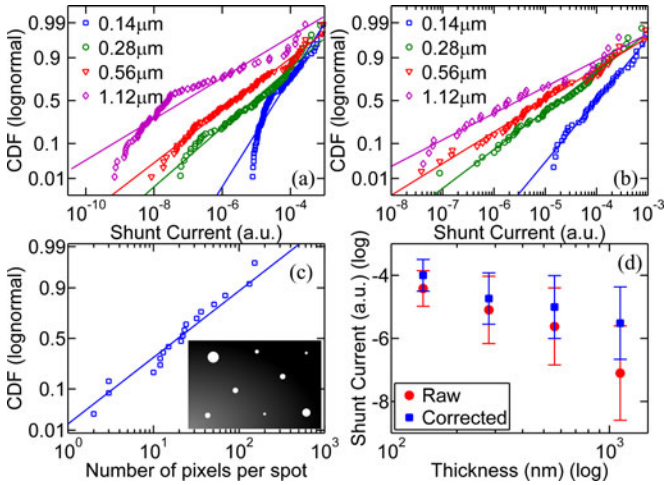

Fig. 6. (a) Lognormal probability of raw $I_{\rm SH}$ data (at -2 V) for four different i-layer thickness (symbols), with best fits (solid lines), shows that the data at 140 and 1120 nm deviates significantly from lognormal. (b) Removing the data points that are contaminated by diode leakage results in much better fit to lognormal behavior for all i-layer thicknesses. (c) Spot size distribution from a reverse bias dark thermography image from [18] (schematic in the inset) also shows a lognormal behavior. (d) The inverse power-law thickness dependence of $I_{\rm SH}$ is preserved after correcting for diode leakage, but the power exponent reduces to -1.6 from -2.8 for the raw data.

[see Fig. 6(b)]. Note that the exact nature of the distribution of shunt magnitude is irrelevant to the overall analysis that is presented so far. Nevertheless, we would like to point out some interesting correlations and qualitative insights from the statistics.

For example, we find the same lognormal distribution for the light-spot size distribution of dark thermography image from [18] [see Fig. 6(c)]. Since the size of spots in the thermography images is proportional to shunt current magnitudes, the lognormal spot size distribution provides an independent confirmation of the lognormal $I_{\rm SH}$ distribution observed from our dark IV measurements. From the p–i–p shunt picture, we know that $I_{\rm SH} \sim A_{\rm shunt}/L^{2\gamma+1}$; therefore, the spread in $I_{\rm SH}$ is attributed to a combination of spread in the area and thickness. Note, however, that the p–i–p model predicts only small Al incursion [see Fig. 4(a)], and consequently, the statistical spread in L for a particular i-layer thickness should be small. This is also apparent from Fig. 6(d), in which we show that the distribution scales with L as a power law very closely. Therefore, we can conclude that the lognormal $I_{\rm SH}$ distribution is a consequence of the lognormal distribution of shunt areas.

This lognormal distribution of the $I_{\rm SH}$ magnitude and spot size distribution gives interesting insights into the problem of shunt conduction. The lognormal distribution means that the largest shunt (lowest resistance) in a particular cell will dominate the total shunt current. Equivalently, the second largest shunt path in a particular cell would be 1–2 orders of magnitude smaller than the largest one. This observation has important implications for understanding of nonvolatile switching in the shunt current as discussed next. Moreover, at the panel level, the lognormal distribution in the $I_{\rm SH}$ magnitude implies that only a handful of the largest shunts will dominate the total shunt loss. Therefore, this analysis tells us that a better strategy for reducing shunt losses at panel level is to selectively remove few largest shunts, instead of a general shunt-busting approach for all cells.

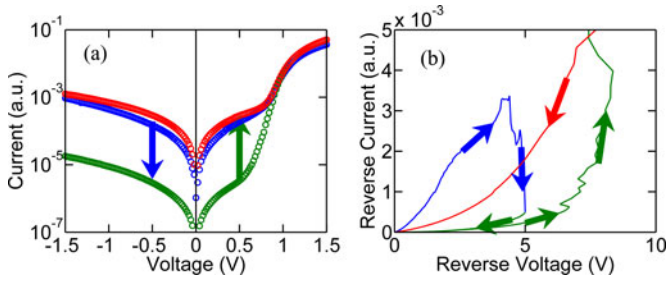

Fig. 7. (a) Initial dark *IV* characteristic (green) switches to the low $I_{\rm SH}$ state after voltage sweep (blue) and increases again after subsequent current sweep (red). (b) Abrupt switching transitions during voltage sweep showing the OFF transition (blue) and current sweep showing the ON transition (red).

V. Nonvolatile Switching

So far, we have showed that the proposed p–i–p shunt model with the SCL shunt current can explain the features of preexisting shunts in a coherent manner. We now discuss how this picture can also help us in understanding the nonvolatile switching in $I_{\rm SH}$ caused by moderate reverse biases.

Threshold switching of shunts in a-Si:H solar cells, under reverse bias, has been reported in the literature and is used in industry for "shunt busting" [8]. However, our measurements show that this switching is actually *metastable*. That is to say that the shunt current of a cell can decrease or *increase* on application of reverse bias. We observe that during reverse voltage sweep, $I_{\rm SH}$ decreases abruptly by about 1–2 orders of magnitude (OFF transition), analogous to the shunt busting [see Fig. 7(a)]. This change in the shunt current is nonvolatile during subsequent *IV* measurements. However, $I_{\rm SH}$ increases again (ON transition), after a subsequent reverse current sweep, and stays at the higher value thereafter. The abrupt transitions of $I_{\rm SH}$ during the two sweeps are shown in Fig. 7(b). Both these metastable states of the shunt current are nonvolatile and remain stable for many days under room temperature storage. In the following sections, we present data and simulations to show that the abrupt switching in the shunt-current magnitude is *not* because of metastability in a single shunt path but a consequence of the shunt formation physics and their statistical distribution.

A. Switching Thresholds for ON and OFF Transitions

In order to investigate the physical features of this switching behavior, we measured 16 nominally identical devices under reverse voltage and current stress. Consecutive voltage sweeps of -5, -6, and -7 V, and reverse current sweeps of 0.5, 5, and 50 mA were applied to all devices. Eight devices were subjected first to voltage sweeps followed by the current sweeps, and the other eight were stressed in the opposite order. The sweep rate was kept at the fastest possible, with the typical sweep time below 1 s (i.e., >10 V/s).

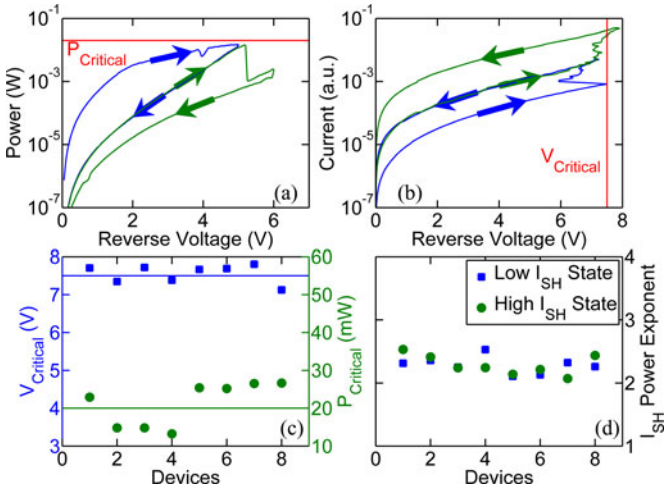

Fig. 8. Reverse bias sweep for a cell with metastable shunt showing that (a) OFF transition is triggered at the power threshold P_{Critical}, for two subsequent voltage sweeps, while (b) ON transition is triggered at the threshold voltage V_{Critical} for two subsequent current sweeps. (c) Scatter plot showing that the values of P_{Critical} and V_{Critical} are similar for eight devices. (d) Power exponent of the SCL shunt current β, in the high (after ON) and low (after OFF) shunt current states remains close to 2.5 showing that the SCL nature of shunt is preserved during the nonvolatile switching.

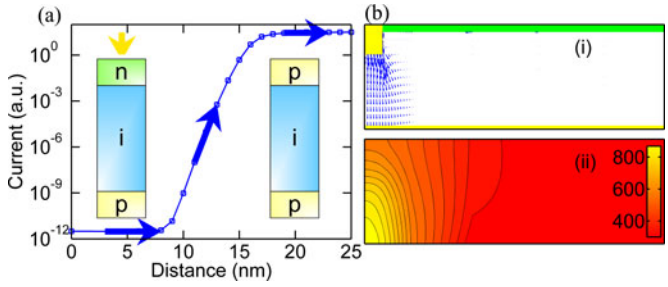

Fig. 9. (a) Simulation showing the change in reverse current at the location of shunt formation, as a function of distance of Al incorporation. As Al gets past the 20-nm n-layer, the current changes significantly (schematics in the inset). (b) Self-consistent simulations of the 2-D shunt structure at reverse bias of −7.5 V, showing (i) localized shunt current and (ii) local heating effect (temperature scale in Kelvins) caused by the fast reverse sweep.

Of the 16 devices measured, eight did not exhibit any switching transition in I_{SH}. For the other eight, which show metastability, the switching showed distinct dependences for ON and OFF transitions. We found that the decrease in I_{SH} (OFF transition) was determined by a power threshold P_{Critical} [see Fig. 8(a)], and the increase in I_{SH} (ON transition) was triggered at a threshold voltage V_{Critical} [see Fig. 8(b)]. These thresholds were independent of the order of the sweeps (i.e., first voltage and then current, or *vice versa*). In Fig. 8(c), we show that the threshold voltage and power values for all the eight metastable shunts are ~ -7.5 V and ~ 20 mW, respectively. Finally, in Fig. 8(d), we compare the SCL power exponent β of the shunt current in high- and low-current states, respectively, showing them to be roughly identical. This shows that the nature of I_{SH} shunts does not change before and after switching.

B. *Mechanism of* ON *Transition*

The robust trends that are observed in our measurements show that this metastability in I_{SH} is indeed a physical feature of shunt conduction. We now discuss how one can understand the metastable switching behavior, using the p–i–p shunt picture developed earlier. First, note that the ON transition is a voltage (analogously electric field)-driven process, as seen in Fig. 8(b). These observations suggest that the positively charged Al ions might be hopping through the a-Si:H matrix under the influence of the electric field and migrating into the a-Si:H layer. Second, we know, from Section II, that only a small Al incursion of ~ 20 nm is sufficient to create the local shunt. As Al gets past the thin n-layer, it will destroy the n–i junction locally and form a p–i–p shunt. Hence, the ON transition (driven by large voltage) would be very rapid, as observed in Fig. 7(b). In Fig. 9(a), we show the change in reverse current versus the distance of Al incorporation in a-Si:H, showing that even a small Al incorporation is sufficient to induce large change in the reverse current.

The voltage-driven contact metal migration in a-Si:H has been studied extensively in nonvolatile resistive switching memories made from a-Si. This in fact forms the basis of operation of the a-Si:H resistive RAM [19]. Direct evidence for Al migration in a-Si:H matrix under bias is also available in the memory literature [20]. Because of the similarities in materials (Al/a-Si:H) and the structures involved, it seems very likely that the similar physical processes are also driving the ON transitions in metastable shunts.

There is, however, an important distinction between the resistive memories and shunt metastability. In the case of a-Si:H-based memories, the program/WRITE electric fields are substantially higher and the conduction is *Ohmic* in the ON state. This is because, in memories, the metal migrates all the way through the bulk and forms a metallic filament [20]. However, for I_{SH}, we observe that I_{SH} power exponent β remains close to 2 before and after the ON transition, as seen in Fig. 8(d). This means that the shunt current continues to be SCL before and after the ON/OFF transition. Therefore, it appears that during the ON transition for I_{SH}, only a small incursion of the metal ions inside the bulk takes place (enough to overcome the n–i junction). Moreover, the shunt-current values after one ON and OFF transition are not necessarily the same. Based on this, we propose that the ON transition happens because of the formation of a *new* shunt path because of Al migration from the top AZO contact.

C. *Mechanism of* OFF *Transition*

Unlike the ON transition, the OFF transition is controlled by a power threshold, as seen in Fig. 8(a). This suggests that the most probable cause of the OFF transition is the dissolution of the small Al filament because of local heating. We discussed, in Section IV, that the largest shunt path in a cell carries most of the current. Moreover, since the sweep rates are high, the local heating at the largest shunt can be significant. In order to check this hypothesis, we simulated the 2-D shunt structure in Fig. 2(b) under moderate reverse bias. In Fig. 9(b), we show the

result of the complete simulation of electron–hole continuity equations that are coupled with the heat equation using Medici TCAD software. The reported values of a-Si:H thermal conductivity and heat capacity were used for the simulation [14]. Note that because of the localization of shunt current in reverse bias, the local temperature can increase by 300–400 °C. While the exact temperature rise will depend on many other factors including the thermal properties of the contacts, which are not included in these simulations; this simulation demonstrates that the temperature rise can be significant. Therefore, it is likely that the largest Al filament might dissolve/disperse at these temperatures, resulting in the OFF transition. And, due to the lognormal distribution of shunt magnitudes, the total current is then determined by the next largest shunt, which is 1–2 orders of magnitude lower than the original shunt current, resulting in the OFF transition.

In summary, our data and analysis show that the OFF transition in shunt switching is related to local heating, and the ON transition is related to Al-ion migration with the electric field. While further measurements are needed to identify the exact mechanism, we have constructed a consistent picture for shunt metastability based on the physics of resistive switching memories and the statistical distribution of preexisting shunts. It appears that the understanding of the physical processes of metal incorporation in the a-Si:H matrix is key to understanding shunt formation in a-Si:H solar cells, and the metastability that is analyzed here can provide important insights for such studies.

We also note that the metastable behavior of shunt currents has also been observed in CdTe cells [21]. Since the SCL shunt model has been shown to be applicable to CIGS cells [22], and given the similar structures of CIGS and CdTe cells, the model that is developed here could in principle be extended to shunts in these cells as well.

VI. Conclusion

A physics-based model of shunt conduction has been developed and validated, which can explain the electrical and metastable features of shunts in a-Si:H p–i–n solar cells. A physical understanding of shunt behavior enables one to explore possible solutions for shunting problems. For example, since Al migration appears to cause shunt formation, it might be useful to put a barrier layer between AZO and a-Si:H to block this migration. Moreover, the understanding of the metastable shunt behavior will enable a better understanding of the degradation of panel performance over time, which is caused by the formation of new shunt paths. For example, the voltage-triggered I_{SH} increase suggests that techniques for avoiding large reverse voltages, which are caused by partial panel shading, would be very important to avoid shunt degradation during the panel operation. While further experiments are needed for the construction of a complete picture of shunt physics, the model that is presented here should provide useful guidance for any such investigations in the future.

Acknowledgment

The authors would like to thank Dr. M. Frei and Dr. D. Wang for helpful discussions and support.

References

[1] K. L. Chopra, P. D. Paulson, and V. Dutta, "Thin-film solar cells: An overview," *Prog. Photovolt., Res. Appl.*, vol. 12, pp. 69–92, 2004.

[2] V. G. Karpov, A. D. Compaan, and D. Shvydka, "Effects of nonuniformity in thin-film photovoltaics," *Appl. Phys. Lett.*, vol. 80, pp. 4256–4258, 2002.

[3] G. T. Koishiyev and J. R. Sites, "Effect of shunts on thin-film CdTe module performance," in *Proc. Mater. Res. Soc. Symp.*, San Francisco, CA, 2009, pp. 203–208.

[4] K. Bothe, K. Ramspeck, D. Hinken, C. Schinke, J. Schmidt, S. Herlufsen, R. Brendel, J. Bauer, J. M. Wagner, N. Zakharov, and O. Breitenstein, "Luminescence emission from forward- and reverse-biased multicrystalline silicon solar cells," *J. Appl. Phys.*, vol. 106, pp. 104510–104518, 2009.

[5] S. Dongaonkar, K. Y, D. Wang, M. Frei, S. Mahapatra, and M. A. Alam, "On the nature of shunt leakage in amorphous silicon p–i–n solar cells," *IEEE Electron Device Lett.*, vol. 31, no. 11, pp. 1266–1268, Nov. 2010.

[6] T. J. McMahon and M. S. Bennett, "Metastable shunt paths in a-Si solar cells," *Solar Energy Mater. Solar Cells*, vol. 41–42, pp. 465–473, 1996.

[7] K. R. Lord, M. R. Walters, and J. R. Woodyard, "Investigation of shunt resistances in single-junction A-Sih alloy solar cells," in *Proc. Mater. Res. Soc. Symp.*, Pittsburgh, PA, 1994, pp. 729–734.

[8] G. E. Nostrand and J. J. Hanak, "Method of removing the effects of electrical shorts and shunts created during the fabrication process of a solar cell," U.S. Patent 4 166 918, RCA Corp., New York, NY, 1979.

[9] S. Dongaonkar, Y. Karthik, D. Wang, M. Frei, S. Mahapatra, and M. A. Alam, "Identification, characterization and implications of shadow degradation in thin film solar cells," in *Proc. IEEE Int. Rel. Phys. Symp.*, 2011, pp. 5E.4.1–5E.4.5.

[10] A. Rose, "Space-charge-limited currents in solids," *Phys. Rev.*, vol. 97, pp. 1538–1544, 1955.

[11] M. Lundstrom, *Fundamentals of Carrier Transport*. Cambridge, U.K.: Cambridge Univ. Press, 2000.

[12] O. Kunz, J. Wong, J. Janssens, J. Bauer, O. Breitenstein, and A. G. Aberle, "Shunting problems due to sub-micron pinholes in evaporated solid-phase crystallised poly-Si thin-film solar cells on glass," *Prog. Photovolt., Res. Appl.*, vol. 17, pp. 35–46, 2009.

[13] M. S. Haque, H. A. Naseem, and W. D. Brown, "Aluminum-induced degradation and failure mechanisms of a-Si:H solar cells," *Solar Energy Mater. Solar Cells*, vol. 41–42, pp. 543–555, 1996.

[14] E. Eser, K. R. Ramaprasad, H. Volltrauer, F. Ramos, S. C. Gau, and R. Vos, "Long-term stability of amorphous silicon solar cells and modules," *Solar Cells*, vol. 21, pp. 25–39, 1987.

[15] F. Schauer and O. Zmeskal, "Temperature dependent SCLC in amorphous silicon," *J. Non-Crystalline Solids*, vol. 164–166, pp. 537–540, 1993.

[16] R. A. Street, *Hydrogenated Amorphous Silicon*. Cambridge, U.K.: Cambridge Univ. Press, 1991.

[17] R. A. Street, "Long-time transient conduction in a-Si:H p–i–n devices," *Philosoph. Mag. B*, vol. 63, pp. 1343–1363, 1991.

[18] V. Sittinger, F. Ruske, W. Werner, B. Szyszka, B. Rech, J. Hüpkes, G. Schöpe, and H. Stiebig, "ZnO:Al films deposited by in-line reactive AC magnetron sputtering for a-Si:H thin film solar cells," *Thin Solid Films*, vol. 496, pp. 16–25, 2006.

[19] A. E. Owen, P. G. L. Comber, J. Hajto, M. J. Rose, and A. J. Snell, "Switching in amorphous devices," *Int. J. Electron.*, vol. 73, pp. 897–906, 1992.

[20] J. W. Seo, S. J. Baik, S. J. Kang, Y. H. Hong, J.-H. Yang, L. Fang, and K. S. Lim, "Evidence of Al induced conducting filament formation in Al/amorphous silicon/Al resistive switching memory device," *Appl. Phys. Lett.*, vol. 96, pp. 053504–053504-3, 2009.

[21] T. J. McMahon, T. J. Berniard, and D. S. Albin, "Nonlinear shunt paths in thin-film CdTe solar cells," *J. Appl. Phys.*, vol. 97, pp. 054503–054503-5, 2005.

[22] S. Dongaonkar, J. D. Servaites, G. M. Ford, S. Loser, J. Moore, R. M. Gelfand, H. Mohseni, H. W. Hillhouse, R. Agrawal, M. A. Ratner, T. J. Marks, M. S. Lundstrom, and M. A. Alam, "Universality of non-Ohmic shunt leakage in thin-film solar cells," *J. Appl. Phys.*, vol. 108, pp. 124509–124509-10, 2010.

Sourabh Dongaonkar received the B.Tech. degree in electrical engineering from the Indian Institute of Technology Kanpur, India, in 2007.

During 2007–2008, he was with the Global Market Center, Deutsche Bank, Mumbai, India, as a quantitative analyst. Since 2008, he has been a graduate student with the School of Electrical and Computer Engineering, Purdue University, West Lafayette, IN. His research interests lie in the areas of thin film solar cells and transport in amorphous and random materials.

Mr. Dongaonkar received the 2008 Ross Fellowship from Purdue University Graduate School.

Karthik Y received the B.Eng. degree in electronics and communication from Sri Jayachamarajendra College of Engineering, Mysore, India, in 2007. He is currently working toward the Master of Technology degree in microelectronics with the Electrical Department, Indian Institute of Technology, Bombay, India.

After completing the bachelor degree, he was with the Microelectronics Lab, Electrical and Computer Engineering Department, Indian Institute of Science, Bangalore, as a Project Assistant during 2007–2008. Currently, he is a Graduate Research Assistant with the Electrical Department, Indian Institute of Technology, Bombay. His research interests are semiconductor device physics, characterization, simulation, and modeling of new and innovative materials and semiconductor devices for various applications.

Souvik Mahapatra (M'02–SM'07) received the Ph.D. degree in electrical engineering from the Indian Institute of Technology (IIT) Bombay, Mumbai, India, in 1999.

During 2000 to 2001, he was with Bell Laboratories, Murray Hill, NJ. Since 2002, he has been with the Department of Electrical Engineering, IIT Bombay, where he presently holds the position of Professor. He has published more than 85 papers in peer-reviewed journals and conferences, delivered invited talks at leading international conferences in the U.S., Europe, and Asia-pacific, including at the IEEE IEDM, delivered reliability tutorials at the IEEE IRPS, and acted as a Reviewer of several international journals and conferences. His research interests are in the area of characterization, modeling and simulation of CMOS and Flash memory devices, and device reliability. He also holds an honorary graduate faculty position with Purdue University, West Lafayette, IN.

Dr. Mahapatra is a Distinguished Lecturer of the IEEE Electron Devices Society.

Muhammad Ashraful Alam (M'96–SM'01–F'06) received the B.S.E.E. degree from Bangladesh University of Engineering and Technology, Dhaka, Bangladesh, in 1988, the M.S. degree from Clarkson University, Potsdam, NY, in 1991, and the Ph.D. degree from Purdue University, Lafayette, IN, in 1994, all in electrical engineering.

He is currently a Professor of electrical and computer engineering with the School of Electrical Engineering and Computer Science, Purdue University, where his research and teaching focus on physics, simulation, characterization, and technology of classical and novel semiconductor devices. From 1995 to 2001, he was with Bell Laboratories, Lucent Technologies, Murray Hill, NJ, as a Member of Technical Staff with the Silicon ULSI Research Department. From 2001 to 2003, he was a Distinguished Member of Technical Staff and the Technical Manager of the IC Reliability Group, Agere Systems, Murray Hill. In 2004, he joined Purdue University. His current research interests include stochastic transport theory of oxide reliability, transport in nanonet thin-film transistors, and nanobio sensors. He has published more than 90 papers in international journals and has presented many invited and contributed talks at international conferences.

Dr. Alam was the recipient of the IRPS Best Paper Award in 2003 and the Outstanding Paper Award in 2001, both for his work on gate oxide reliability, and the IEEE Kiyo Tomiyasu Award for his contributions to device technology for communication systems. Most recently, he was elected IEEE Fellow for his contribution to the physics of CMOS reliability and simulation of optoelectronic devices.